

## Synthesis and evaluation of novel Cu-based adsorbent-containing catalysts for CO<sub>2</sub> hydrogenation to methanol and value-added products

Rim Ismail, Mohamed Ali H. Saad, Mohamed J. Al-Marri, Ali Sardar, Assem T. Mohamed, Muftah El-Naas, Ahmed M.S. Soliman, Abdelbaki Benamor

### Item type

Journal Contribution

### Terms of use

This work is licensed under a [CC BY 4.0](#) license

### This version is available at

[https://manara.qnl.qa/articles/journal\\_contribution/Synthesis\\_and\\_evaluation\\_of\\_novel\\_Cu-based\\_adsorbent-containing\\_catalysts\\_for\\_CO\\_sub\\_2\\_sub\\_hydrogenation\\_to\\_methanol\\_and\\_value-added\\_products/25449601/1](https://manara.qnl.qa/articles/journal_contribution/Synthesis_and_evaluation_of_novel_Cu-based_adsorbent-containing_catalysts_for_CO_sub_2_sub_hydrogenation_to_methanol_and_value-added_products/25449601/1)

Access the item on Manara for more information about usage details and recommended citation.

Posted on Manara – Qatar Research Repository on

2024-04-01



# Synthesis and evaluation of novel Cu-based adsorbent-containing catalysts for CO<sub>2</sub> hydrogenation to methanol and value-added products

Rim Ismail<sup>a</sup>, Mohamed Ali H. Saad<sup>a,b</sup>, Mohamed J. Al-Marri<sup>a,b</sup>, Ali Sardar<sup>a</sup>, Assem T. Mohamed<sup>a</sup>, Muftah El-Naas<sup>a</sup>, Ahmed M.S. Soliman<sup>a</sup>, Abdelbaki Benamor<sup>a,b,\*</sup>

<sup>a</sup> Gas Processing Center, College of Engineering, Qatar University, Doha 2713, Qatar

<sup>b</sup> Department of Chemical Engineering, College of Engineering, Qatar University, Doha 2713, Qatar

## ARTICLE INFO

Editor: Zacharias Frontistis

### Keywords:

Catalyst  
Copper  
Alumina  
Adsorbent  
CO<sub>2</sub> conversion  
Methanol

## ABSTRACT

In this work, sequential incipient wetness impregnation method was used to synthesize Cu/Al<sub>2</sub>O<sub>3</sub>, Cu/Na<sub>2</sub>O/Al<sub>2</sub>O<sub>3</sub> and Cu/CaO/Al<sub>2</sub>O<sub>3</sub> catalysts in different compositions for CO<sub>2</sub> conversion to value-added products. Synthesized catalysts were characterized using various analytical techniques and their performances for CO<sub>2</sub> catalytic conversion were tested in a high-pressure packed bed reactor under reaction conditions of P = 60 bars, T = 300 °C, and H<sub>2</sub>/CO<sub>2</sub> = 3. The obtained results revealed that the type of adsorbent had a significant impact on CO<sub>2</sub> conversion, with CaO-containing catalyst being more efficient for methanol selectivity. Increased Cu content from 10 wt% to 30 wt% with fixed CaO content of 10 wt% resulted in a small increase in CO<sub>2</sub> conversion where the highest CO<sub>2</sub> conversion of 16.44% and the highest methanol selectivity (17.75%) were obtained for catalyst containing 20 wt% of copper. The best performing catalyst was further promoted using 0.5 wt% Rh promoter which improved both methanol selectivity and space time yield to 23.2% and 0.08 g<sub>MeOH</sub>g<sub>cat</sub><sup>-1</sup>h<sup>-1</sup>, respectively. The comparative high performance of the Rh-promoted catalyst was attributed to smaller metal oxide particle size with uniform dispersion, presence of effective hydrogen spill over, moderate basic sites, surface defects and presence of induced copper species.

## 1. Introduction

The surge in energy demand over recent decades, driven by rapid population growth and economic expansion, has become a prominent global challenge. This heightened demand, largely met by fossil fuels, poses significant environmental concerns on a global scale. The predominant issue stems from the associated emissions of greenhouse gases (GHGs), contributing to phenomena such as global warming and climate change. Fossil fuel combustion is a major contributor to GHGs, with carbon dioxide (CO<sub>2</sub>) experiencing the most substantial annual increase, reaching approximately 2.4 ppm/year. This escalating trend paints a concerning picture of rising CO<sub>2</sub> concentrations in the Earth's atmosphere [1] as it is expected that the CO<sub>2</sub> level will surpass a catastrophic concentration limit of 570 ppm by the end of 21st century if no proper CO<sub>2</sub> abatement policies are implemented [2]. CO<sub>2</sub> emissions are thought to be the main reason for the associated rising temperature of the earth's average surface expected to lay between 1.4 and 5.8 °C in 2100 [3], accelerating climate change phenomena that causes long-lasting

consequences and ecological imbalance [4,5]. Hence, developing new technologies to reduce carbon emissions is very crucial towards CO<sub>2</sub> mitigation.

Several options have been adopted for CO<sub>2</sub> mitigations such as carbon capture and storage (CCS) that has been employed to reduce CO<sub>2</sub> emissions in the atmosphere by injecting capture CO<sub>2</sub> into geological sites or dissolving it in deep oceans; however this option has the risk of increasing ocean acidifications, and with the rise in CO<sub>2</sub> concentration, net CO<sub>2</sub> uptake eventually will decrease in oceans [2]. Recently, CO<sub>2</sub> conversion has been considered as a possible CO<sub>2</sub> mitigation route especially at point sources where CO<sub>2</sub> emissions with high concentration can be used as carbon source to produce valuable hydrocarbons via catalytic conversion processes, such as thermal catalysis [6], electrocatalysis [1,7] and photocatalysis [8]. Recently, dual-functional materials (have been investigated for integrated carbon capture and utilization (CCU). The dual-functional materials have a bi-functionality, where adsorbent basic sites directly capture CO<sub>2</sub>, and a catalytic metallic component converts it to value-added products such as methane,

\* Corresponding author at: Gas Processing Center, College of Engineering, Qatar University, Doha 2713, Qatar.

E-mail address: [benamor.abdelbaki@qu.edu.qa](mailto:benamor.abdelbaki@qu.edu.qa) (A. Benamor).

<https://doi.org/10.1016/j.jece.2024.112325>

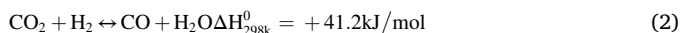
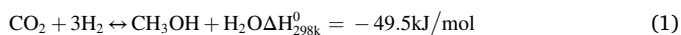
Received 18 November 2023; Received in revised form 22 February 2024; Accepted 23 February 2024

Available online 28 February 2024

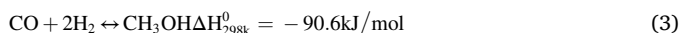
2213-3437/© 2024 The Author(s). Published by Elsevier Ltd. This is an open access article under the CC BY license (<http://creativecommons.org/licenses/by/4.0/>).

methanol...etc. Targeting CO<sub>2</sub> hydrogenation to methanol using renewable hydrogen is a promising environmental-friendly pathway to reduce CO<sub>2</sub> emissions. Methanol is one of the top five shipped chemicals worldwide. Methanol is a primary raw material, and valuable chemical in industry that can be utilized directly as fuel or indirectly as intermediate in the production of other value-added products including formaldehyde, acetic acid, and biodiesel [9].

Three processes represent the methanol synthesis by CO<sub>2</sub> hydrogenation. The methanol synthesis as per reactions (1) and (3), are exothermic, and the RWGS described in reaction (2), is the major competitive reaction in the process of CO<sub>2</sub> hydrogenation to methanol [10]:



The CO formed via RWGS is likely to be hydrogenated to methanol as per reaction (3) [2].



Solid adsorbents for CO<sub>2</sub> capture had a great deal of attention from researchers owing to their characteristics including their wide range of operating temperatures (25–700 °C), easiness to handle and dispose with less environmental issues. Different adsorbing materials were developed for CO<sub>2</sub> capture including zeolites [11], metal organic frameworks (MOFs) [3,12], mesoporous materials and activated carbon [13]. Although they showed high affinity towards CO<sub>2</sub>, their adsorption capacity is significantly influenced by the elevated temperature [14]. Several characteristics of the sorbent material are required to achieve quality CO<sub>2</sub> adsorption performance such as high adsorption capacity, higher selectivity towards CO<sub>2</sub> over the gas stream components (e.g. N<sub>2</sub>, H<sub>2</sub>), rapid sorption rate, high mechanical strength, chemical/thermal stability, and low-cost [15]. Long-term exposure of the adsorbent to the flue gas at high temperature may affect its stability and performance due to sintering. To resolve this issue, several workers [16,17] mixed the adsorbent with a carrier material acting as a support material, which results in a higher surface area and better adsorbent dispersion with enhanced stability derived from the highly dispersed adsorbent. Metallic oxide sorbents for CO<sub>2</sub> are well-documented in the literature and used for CO<sub>2</sub> capture owing to the ease of interaction between their high surface basic sites and the acidic CO<sub>2</sub> species. Feng et al. screened a series of metal-oxide sorbents and reported their CO<sub>2</sub> uptake capacity and the energy required for their regeneration [18]. Among the evaluated sorbents, MgO and CaO exhibited the highest capture capacity. Na<sub>2</sub>O exhibited relatively good performance with a CO<sub>2</sub> capacity of 0.709 g CO<sub>2</sub>/g sorbent even at temperatures above 927 °C.

Considering that alumina is a weak basic material, introducing Al<sub>2</sub>O<sub>3</sub> as support for alkali-metal oxides like sodium oxide is expected to display good CO<sub>2</sub> adsorption capacity even at high temperatures [19]. The CO<sub>2</sub> adsorption-desorption over Na<sub>2</sub>O/Al<sub>2</sub>O<sub>3</sub> was investigated by Keturakis et al. [4,20]. Their study revealed that doping Na<sub>2</sub>O on Al<sub>2</sub>O<sub>3</sub> decomposed Na<sub>2</sub>O to an ionic form, enabling CO<sub>2</sub> to be adsorbed on both Al<sub>2</sub>O<sub>3</sub> sites via interaction between CO<sub>2</sub> and -OH groups or on Na<sub>2</sub>O sites where CO<sub>2</sub> is adsorbed on Na<sub>2</sub>O sites to form bidentate carbonates. Doping metal-oxide-based adsorbents including CaO, K<sub>2</sub>O, Na<sub>2</sub>O, and MgO into γ-Al<sub>2</sub>O<sub>3</sub> was investigated by Arellano et al. [21]. The highest CO<sub>2</sub> adsorption was reported for Na<sub>2</sub>O- Al<sub>2</sub>O<sub>3</sub> (650 mmol/kg-cat) and CaO- Al<sub>2</sub>O<sub>3</sub> (681.5 mmol CO<sub>2</sub>/kg-cat). However, the use of Na<sub>2</sub>O is limited by its high regeneration energy. at the opposite of CaO-based adsorbent that proved to be much more cost effective than the conventional amine scrubbing technologies for CO<sub>2</sub> capture with a costs around 16–44 \$/ton CO<sub>2</sub> against a cost in the range of 32–80 \$/ ton CO<sub>2</sub> for amine based scrubbing technology [22]. Even though CaO has distinctive features that make it one of the most utilized adsorbents, it has some limitations, such as excessive sintering. To reduce this

phenomenon, several strategies have been attempted to improve its stability and reusability including the dispersion of CaO on an inert carrier (e.g. γ-Al<sub>2</sub>O<sub>3</sub>). Belova et al. proved that dispersing CaO on γ-Al<sub>2</sub>O<sub>3</sub> increases the surface area of CaO particles, thus improving the CaO sorption capabilities and reducing the sintering effect [23]. Furthermore, it was demonstrated that CaO/γ-Al<sub>2</sub>O<sub>3</sub> acts as an excellent reversible adsorbent at temperatures falling in the range of 300–650 °C, which is high enough to perform and proceed with CO<sub>2</sub> catalytic reaction [24]. Moreover, CaO/γ-Al<sub>2</sub>O<sub>3</sub> can be easily synthesized via the common preparation techniques used in the catalyst industry.

Active metals such as Cu, Pd, Ni, and others, impregnated over different supports have been investigated for CO<sub>2</sub> conversion over the last decades. Cu-based catalysts represent the majority of employed catalysts due to their good performances such as high CO<sub>2</sub> conversion, high methanol yield, and high selectivity. Although the active site nature and valence of copper are still debatable, it is well-known that copper serves as an active catalyst either in its Cu<sup>0</sup> or Cu<sup>+</sup> nature. In CO<sub>2</sub> conversion reactions to methanol over a Cu based catalyst, there are two main reactions that take place over the Cu surface. In the first one, carbon dioxide is coordinated, chemisorbed, and activated, while the second one refers to hydrogen homogeneous splitting [25]. Moreover, it was pointed out that the material activity and CO<sub>2</sub> hydrogenation are directly proportional to the metallic Cu surface area. Generally, there is an agreement that the core function of copper is to offer an active site, where H<sub>2</sub> dissociation takes place [26]. Promoted catalysts for methanol synthesis still remain in their investigation stage and need in-depth investigations related to the cost and STY before being applied at industrial level. Different concepts have been put forward to facilitate and enhance the thermo-catalytic activity of the catalyst, one of which is introducing a second metal or noble metal into copper. Several researchers have demonstrated that this approach would modify the electron structure and enhances the activity of methanol synthesis catalysts [27]. Nevertheless, promoting Cu-based catalyst by introducing a noble metal eventually results in a convenient adjustment in the electronic property of the catalyst [28]. Several precious metal-based promoters have been reported to increase the production of methanol from the hydrogenation of carbon dioxide [5–9]. Among them, catalysts based on rhodium that have received a lot of attention recently because of their wide range of applications in hydrogenation processes with CO<sub>2</sub> as the reactant. The utilization of Rh-based materials for heterogeneous and homogeneous catalysts in a number of catalytic applications has been the subject of numerous articles [10–13]. For instance, Rh was shown to improve hydrogen spillover and dispersion, which in turn led to an increase in methanol production and selectivity when incorporated into In<sub>2</sub>O<sub>3</sub>-based catalysts [14]. It has been proposed that the incorporation of Rh in the catalyst composition promotes hydrogen spill over by facilitating in the dissociative adsorption of hydrogen molecules. Moreover, employing Rh as a catalyst or promoter accelerates the adsorption of reaction intermediates during the CO<sub>2</sub> hydrogenation step of the methanol synthesis process, enhancing the yield of methanol [15].

In the present work, we aimed at synthesizing a novel and highly active Cu-based catalyst for CO<sub>2</sub> hydrogenation to methanol and other value-added products. copper was chosen as catalytic active component that facilitates hydrogen adsorption and spill over, whereas, CaO and Na<sub>2</sub>O were selected as effective adsorbents dispersed over Al<sub>2</sub>O<sub>3</sub> support. The performances of the novel catalysts were compared to bare Cu/Al<sub>2</sub>O<sub>3</sub> catalyst to explore the effect of adsorbent addition on the CO<sub>2</sub> conversion reaction. The effects of incorporation of Rh in the best performing catalyst as a promoter was further investigated in this work.

## 2. Experimental

### 2.1. Chemicals

Chemicals used in this work were alumina (γ-Al<sub>2</sub>O<sub>3</sub> PURLOX TH100/150) obtained free of charge from SASOL, USA. Sodium carbonate

( $\text{Na}_2\text{CO}_3$ , 99% purity) was purchased from Fluka chemical, Germany. Aqueous precursor solutions of calcium nitrate tetrahydrate, ( $\text{Ca}(\text{NO}_3)_2 \cdot 4 \text{H}_2\text{O}$ , 99w%) was purchased from BDH, UK, while copper nitrate trihydrate ( $\text{Cu}(\text{NO}_3)_2 \cdot 3 \text{H}_2\text{O}$ , 99%) was purchased from Research Lab Fine Chem industries, India. Rhodium (III) nitrate, ( $(\text{RhNO}_3)_3$ , 36%), was purchased from Alfa Aesar, USA. All chemicals used in this study were used as received without further purification. Deionized water was used throughout the experiments.

## 2.2. Catalyst synthesis

All catalysts were synthesized via the sequential incipient wetness impregnation method [29]. Initially, Copper loading of 30 wt% was impregnated on  $\gamma\text{-Al}_2\text{O}_3$  support. Various loading of the adsorbents, i.e., 5 wt%CaO, 10 wt%CaO, and 10 wt% $\text{Na}_2\text{O}$  were impregnated on the carrier  $\gamma\text{-Al}_2\text{O}_3$ . For this purpose, required amount of alumina was degassed overnight in vacuum at  $120^\circ\text{C}$ . The required amounts of the adsorbents ( $\text{Ca}(\text{NO}_3)_2 \cdot 3 \text{H}_2\text{O}$ ) or ( $\text{Na}_2\text{CO}_3$ ) were dissolved in deionized water based on the pore volume of alumina and added dropwise to the degassed alumina with continuous stirring. The resultant slurry was dried at  $140^\circ\text{C}$  for 12 hours followed by calcination in a muffle furnace at  $500^\circ\text{C}$  for two hours at a heating rate of  $5^\circ\text{C}/\text{min}$ . A schematic representation of the synthesis procedure is given in Fig. 1. Copper (Cu) based catalysts with different compositions were synthesized using copper nitrate hexahydrate ( $\text{Cu}(\text{NO}_3)_2 \cdot 6 \text{H}_2\text{O}$ ) as precursor. Aqueous solution of ( $\text{Cu}(\text{NO}_3)_2 \cdot 6 \text{H}_2\text{O}$ ) was added dropwise with constant stirring on the adsorbent  $\text{Na}_2\text{O}/\text{Al}_2\text{O}_3$  or  $\text{CaO}/\text{Al}_2\text{O}_3$  powders. The obtained Cu-based materials were then air-dried at  $140^\circ\text{C}$  overnight and further calcined in air at  $500^\circ\text{C}$  for 2 h hrs. The best performing catalyst was chosen and promoted with 0.5% rhodium using Rhodium(III) nitrate, ( $(\text{RhNO}_3)_3$  36%), as precursor. The same synthesis procedure was used for the promoted catalyst. A summary of synthesized materials is given in Table 1

## 2.3. Catalysts characterization

Freshly prepared catalysts were characterized using several bulk and surface sensitive analytical techniques such as BET surface area by  $\text{N}_2$  adsorption-desorption measurements, X-ray diffraction (XRD), high-resolution electron microscope (HR-TEM), X-ray photoelectron spectroscopy (XPS) and hydrogen temperature programmed reduction ( $\text{H}_2$ -TPR). BET analysis was used to determine the catalyst pore volume, pore

**Table 1**

The abbreviation of the prepared catalysts and their corresponding compositions.

No.	Prepared catalysts	Abbreviation	Composition, weight %			
			CaO	$\text{Na}_2\text{O}$	Cu	Rh
1	30%Cu/ $\text{Al}_2\text{O}_3$	30Cu	0	0	30	0
2	10%Cu10% $\text{Na}_2\text{O}/\text{Al}_2\text{O}_3$	10Cu10 $\text{Na}_2\text{O}$	0	10	10	0
3	10%Cu10%CaO/ $\text{Al}_2\text{O}_3$	10Cu10CaO	10	0	10	0
4	20%Cu10%CaO/ $\text{Al}_2\text{O}_3$	20Cu10CaO	10	0	20	0
5	30%Cu10%CaO/ $\text{Al}_2\text{O}_3$	30Cu10CaO	10	0	30	0
6	20%Cu5%CaO/ $\text{Al}_2\text{O}_3$	20Cu5CaO	5	0	20	0
7	0.5%Rh20%Cu5%CaO/ $\text{Al}_2\text{O}_3$	0.5Rh20Cu5CaO	5	0	20	0.5

size, and the total surface area. The analysis was carried out in a Micromeritics Tristar II series apparatus. In this experiment, the sample was degassed at  $90^\circ\text{C}$  for 1 hour, then the temperature was raised to  $350^\circ\text{C}$  for 4 hours under flowing high purity nitrogen. Brunauer-Emmett-Teller model was used to measure specific surface area ( $\text{m}^2/\text{g}$ ) of the materials whereas pore volume, pore diameter and pore size distribution were measured using Barrett-Joyner-Halenda model. The structure of the bulk crystalline phase of the catalysts was evaluated by analyzing XRD patterns obtained using a desktop X-ray diffractometer (Rigaku MiniFlex-600 $^\circ$ ) instrument. The apparatus was equipped with Cu K $\alpha$  radiation source at 30 kV and 15 mA. Data were collected at a scanning angle ( $2\theta$ ) from  $\sim 5^\circ$  to  $80^\circ$  with a scanning speed of  $4^\circ/\text{min}$ . HR-TEM (TECNAI G2 TEM, TF20) was utilized to corroborate the morphology and particle size of the samples. Samples were prepared by sonicating few mg of the catalyst powder in n-propane and transferring a drop onto a 200-mesh copper grid. The surface chemical compositions of the catalysts were determined by XPS analysis using AXIS Ultra DLD, Kratos spectrophotometer. Prior to the analysis, the samples surfaces were cleaned using Ar ion gun under an applied voltage of 4 kV. The  $\text{H}_2$ -TPR technique using Chemi-Sorb2750 (Micromeritics) was employed to investigate the reduction behaviour of dispersed supported metal oxides samples. 100 mg of the catalyst sample was placed between two layers of quartz wool in a U-shape quartz tube and degassed at  $200^\circ\text{C}$  for

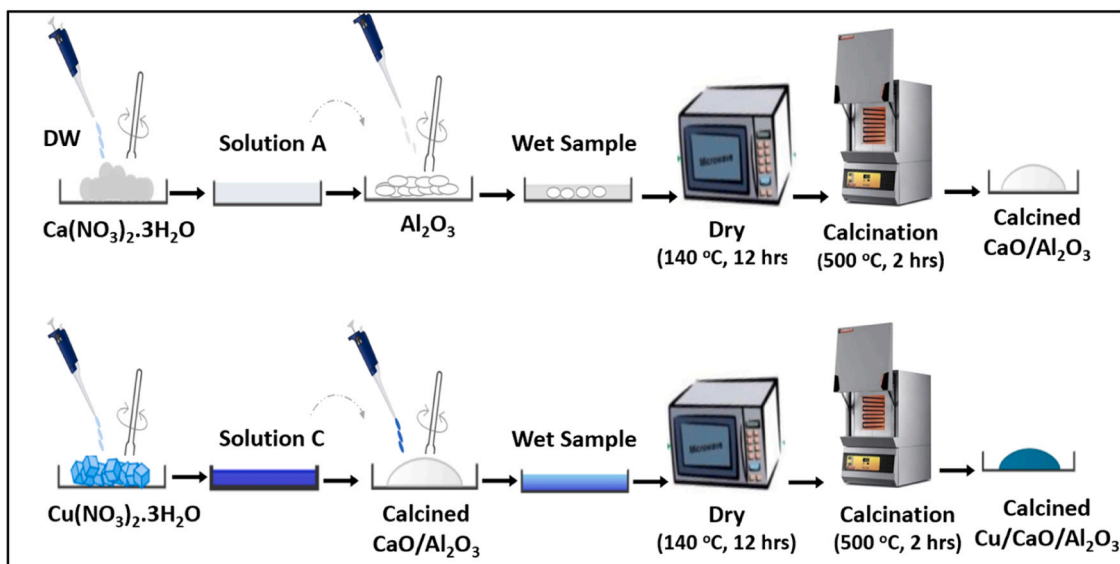


**Fig. 1.** Synthesis procedure of the catalysts.



1 hour under argon flow of 20 ml/min. The temperature was raised to 200 °C at a heating rate of 10 °C/min. The apparatus was then cooled down to 40 °C and the flowing gas switched to a mixture of 5% H<sub>2</sub>/Ar at a flow rate of 25 cm<sup>3</sup>/min. The temperature was then ramped from 40 °C to 800 °C at a heating rate of 10 °C/min. A TCD connected to the tail gas was utilized to determine the amount of consumed hydrogen in the passing gas mixture. The H<sub>2</sub>-TPD technique was employed to investigate the reduction behavior of the samples using Chemisorb2750 (Micromeritics). In this procedure around 100 mg of the sample was loaded into the U-shaped quartz tube by sandwiching it between two layers of quartz wool. Temperature was then ramp from room temperature to 350 °C at a ramp rate of 2 °C/min in the presence of 30 SCCM of 5% H<sub>2</sub>/Ar then it was kept for one hour. This was followed by cooling down to room temperature and removal of access hydrogen by flushing it with pure Ar for twenty minutes. The H<sub>2</sub>-TPD was then recorded by ramping the temperature to 600 °C at a ramp rate of 2 °C/min in the presence of 30 SCCM of pure argon. For the CO<sub>2</sub>-TPD characterization test, around 0.2 g catalyst placed into U shape quartz tube and heated up to 300 °C in 30 SCCM of 5% H<sub>2</sub>/Ar with a dwell time of one hour. The system was cooled down to 50 °C followed by exposure to CO<sub>2</sub> stream 30 ml min<sup>-1</sup> for 1 h, later the system was purged for 30 min with Ar to flush the excess CO<sub>2</sub>. The desorption of chemisorbed CO<sub>2</sub> was achieved by heating up to 800 °C at 10 °C min<sup>-1</sup> under flow of 30 ml min<sup>-1</sup> of Ar.

#### 2.4. Reactor performance tests

Performance evaluation of CO<sub>2</sub> catalytic hydrogenation was performed in a high-pressure lab-scale test unit (PID, Micrometrics) fitted with a hastelloy fixed bed having an internal diameter of 9.3 mm. The reactor tube was placed and heated externally with a three-zone electric furnace, a thermocouple was installed inside the reactor to monitor and control the temperature. High-accuracy mass flow controllers were used to control the gas flow rates. A schematic diagram of the experimental setup is illustrated in Fig. 2. For each test, typically, 500 mg of powdered catalyst was loaded in the middle of the reactor tube sandwiched between two layers of quartz wool. The catalyst pre-reduction was done under pure H<sub>2</sub> flowing at a rate of 20 ml.min<sup>-1</sup> and a temperature of 450 °C with a heating rate of 5 °C min<sup>-1</sup> for two hours. The activated sample was then purged with a flow of 20 ml. min<sup>-1</sup> pure N<sub>2</sub> for five minutes. To start the CO<sub>2</sub> conversion reaction, the reactor temperature was brought down to 300 °C and the feed gas consisting of a mixture of CO<sub>2</sub> and H<sub>2</sub> with ratio of 3:1 flowing at a rate of 60 ml min<sup>-1</sup> was first introduced, followed by increasing the total reactor pressure to 60 bars. Analysis of gaseous products was performed online with a gas chromatograph equipped with a thermal conductivity detector (GC-TCD), whereas the

liquid products collected in a trap (5 °C) were analyzed offline by gas chromatography (GC Agilent 7890) equipped with a flame ionization detector (GC-FID).

The CO<sub>2</sub> hydrogenation conversion over the synthesized catalysts was calculated using Eq. 4:

$$\text{CO}_2\text{conversion}(\%) = \left[ \frac{f_{\text{CO}_2}(\text{in}) - f_{\text{CO}_2}(\text{out})}{f_{\text{CO}_2}(\text{in})} \right] \times 100 \quad (4)$$

Where *f* is the flow rate of gas. The selectivity of the products (methanol, CO, and CH<sub>4</sub>) were calculated using Eqs. 5–7, respectively:

$$\text{CH}_3\text{OH}_{\text{selectivity}}(\%) = \left[ \frac{n_{\text{CH}_3\text{OH}}}{n_{\text{Total product}}} \right] \times 100 \quad (5)$$

$$\text{CO}_{\text{selectivity}}(\%) = \left[ \frac{n_{\text{CO}}}{n_{\text{Total product}}} \right] \times 100 \quad (6)$$

$$\text{CH}_4\text{selectivity}(\%) = \left[ \frac{n_{\text{CH}_4}}{n_{\text{Total product}}} \right] \times 100 \quad (7)$$

Where *n* is the number of moles of the component. The methanol and CO yield in g<sub>P</sub> g<sub>cat</sub><sup>-1</sup> h<sup>-1</sup> were calculated using Eqs. 8 and 9, respectively:

$$\text{CH}_3\text{OH}_{\text{yield}} = \left[ \frac{\text{gCH}_3\text{OH}}{\text{wt of catalyst(g)} \times \text{h}} \right] \quad (8)$$

$$\text{CO}_{\text{yield}} = \left[ \frac{\text{gCO}}{\text{wt of catalyst(g)} \times \text{h}} \right] \quad (9)$$

### 3. Results and discussion

#### 3.1. Material characterization

##### 3.1.1. Catalysts morphology

The morphology and structure of synthesized catalysts were analyzed using HR-TEM as shown in Fig. 3. TEM images were analyzed using ImageJ software to estimate the metal oxide particle size distribution and the average particle size. Fig. 3 shows representative HRTEM images, whereas Figure S1 in the supplementary data shows additional TEM images with particle size distribution histograms. The BET isotherm for nitrogen adsorption-desorption obtained with the synthesized materials are presented in Figure S2. Fig. 3(a) and (b) display the results of 10Cu10Na<sub>2</sub>O and 10Cu10CaO catalysts that contain 10 wt% copper each, and 10 wt% of Na<sub>2</sub>O or CaO adsorbent supported on alumina respectively. Both samples exhibit spherical shaped particles but with different distributions and particle sizes. The particle size of the 10Cu10Na<sub>2</sub>O was relatively higher with an average particle size of 9.35 nm whereas the 10Cu10CaO particle size was smaller with an average size of 8.1 nm. A Summary of obtained results is given in Table 2.

The effect of increased copper oxide loading on the catalyst's morphology was investigated using materials containing 10 wt% CaO and varying metal percentages as shown in Figs. (3b), (3c) and (3d). TEM images of the three different samples showed porous spherical shapes for the three catalysts with a slight increase in the metal oxide particle sizes from 8 nm to 9.23 nm with increased CuO loading from 10 wt% to 20 wt% respectively. However, with further increase in copper oxide loading to 30 wt% in 30Cu10CaO catalyst, a slight decrease in the average particle size to 8.35 nm was observed. It is worth noticing that for the catalyst with increased copper oxide loading Cu metal loading catalyst, a few big particles with a size of 23.5 nm were observed. These particles are most likely the result of nanoparticles agglomeration. At the opposite of other samples, 20Cu5CaO catalyst containing 20 wt% copper oxide (Fig. 3e) clearly shows that the adsorbent is more observable in the sample containing a larger proportion of CaO (Fig. 1c). The TEM image of the 20Cu5CaO exhibited

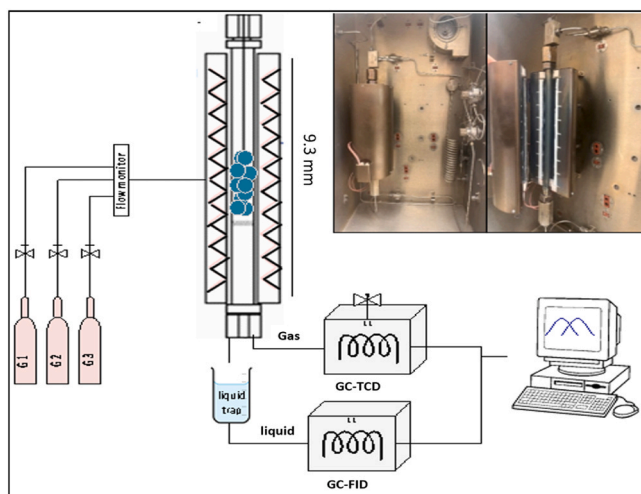


Fig. 2. Schematic diagram of the experimental set-up.

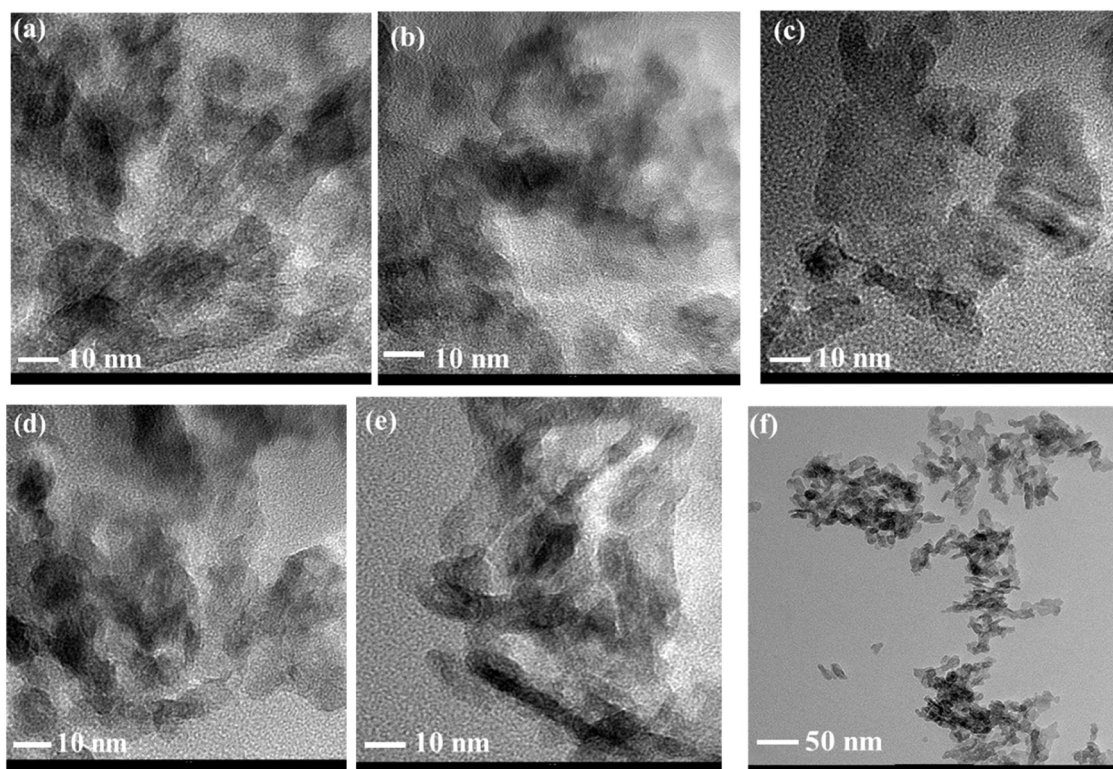


Fig. 3. TEM images of (a) 10Cu10Na<sub>2</sub>O, (b) 10Cu10CaO, (c) 20Cu10CaO, (d) 30Cu10CaO, (e) 20Cu5CaO and (f) 0.5Rh20Cu5CaO.

Table 2

Physical properties of the catalysts and base materials along with their assigned terminology.

No.	Samples	$S_{\text{BET}}$ (m <sup>2</sup> /g)	$V_{\text{pore}}$ (cm <sup>3</sup> /g)	$d_{\text{c,TEM}}$ (nm)
1	$\gamma$ -Al <sub>2</sub> O <sub>3</sub>	150	0.60	-
2	5CaO/ $\gamma$ -Al <sub>2</sub> O <sub>3</sub>	155	0.70	-
3	10CaO/ $\gamma$ -Al <sub>2</sub> O <sub>3</sub>	142	0.60	-
4	30Cu	101	0.60	-
5	10Cu10Na <sub>2</sub> O			9.3
6	10Cu10CaO	126	0.80	8.1
7	20Cu10CaO	108	0.70	9.2
8	30Cu10CaO	90	0.60	8.3
9	20Cu5CaO	107	0.71	7.3
10	0.5Rh20Cu5CaO	107	0.71	7.3

metal oxide particles with a smaller average size of about 7.35 nm. Fig. 3f, shows the corresponding metal oxide particle size distribution of Rh-promoted catalyst. The sample exhibited randomly distributed spherical particles with an average size of 7.3 nm. The 20Cu5CaO catalyst was stable after incorporating Rh, as shown by the small difference in average metal oxide particle size before and after promotion (Table 2).

### 3.1.2. Textural properties of the catalysts

XRD technique was employed to investigate the textural characteristics of the synthesized materials in terms of crystallinity and the existence of different phases. XRD patterns in Fig. 4 shows that alumina (pattern a) had distinct peaks at 2-theta values of 37.5°, 45.7°, and 66.7° with d-spacings of 0.239°, 0.197°, and 0.140°, respectively [30]. Additionally, several small  $\gamma$ -Al<sub>2</sub>O<sub>3</sub> diffraction peaks can be observed at 31.7°, 39.2°, and 60.6° attributed to the (220), (222), and (511) reflection of  $\gamma$ -Al<sub>2</sub>O<sub>3</sub>, respectively [31]. The phase crystallinity and the structural analysis of Cu-containing catalysts represented in Fig. 4 (patterns b-h) exhibited additional peaks corresponding to CuO at 2 $\theta$  of 32.2°, 35.2°, 38.8°, 48.7°, 53.9°, 58.7°, 61.7°, 66.2°, 72.4°, and 75°

which were in line with the results reported by Suresh et al. [32]. The highest crystallinity of CuO was recorded for 30Cu and 30Cu10CaO catalysts with no remarkable difference in peak intensity of CuO peaks since both materials have similar Cu content. 20Cu10CaO has a comparatively higher intensity peak with respect to samples containing 10% Cu impregnated on Al<sub>2</sub>O<sub>3</sub>. the diffractograms revealed that CuO intensity decreased sharply for the samples with the lowest copper loading shown in Fig. 4, (pattern c, d) regardless of the used adsorbent. This can be attributed to the interaction between the metal and the adsorbent in the material surface. The XRD pattern obtained for fresh Rh-promoted catalyst shown in Fig. 4 (pattern h) did not reveal the presence of Rh or Rh oxides, suggesting that the content of Rh species is below the detection limits of XRD apparatus. In all cases, incorporation of the adsorbing material in the catalyst composition did not reveal additional crystalline peaks indicating the presence of highly dispersed Na<sub>2</sub>O and CaO. These findings are in line with other research that have been published [33,34].

The N<sub>2</sub>-adsorption-desorption technique was utilized to estimate surface areas, pores volumes and pores diameters of the synthesized catalysts. All catalysts had type IVa N<sub>2</sub> physisorption isotherms, indicating mesoporous structure of the materials with pore diameters greater than 4 nm. As summarized in Table 2, the addition of 5 wt% CaO to bare Al<sub>2</sub>O<sub>3</sub> increased the  $S_{\text{BET}}$  surface area, indicating excellent dispersion of CaO adsorbent. However, the addition of 10 wt%CaO led to a decrease in alumina SBET from 150 m<sup>2</sup>/g to 142 m<sup>2</sup>/g, most likely as a result of alumina pores blocking. The  $S_{\text{BET}}$  of the 10Cu10CaO, 20Cu10CaO and 30Cu10CaO catalysts were 126 m<sup>2</sup>/g, 108 m<sup>2</sup>/g and 90 m<sup>2</sup>/g, respectively. As expected, catalysts with the lower content of copper had higher surface area and pore volume compared to those with higher copper content, which indicated that they are likely to have better catalytic performances. The pore volumes of the catalyst were lower than those of the substrate materials could be attributed to the deposition of copper metal onto the surface of the materials rather than in its pores, maintaining more vacancies for CO<sub>2</sub> adsorption.

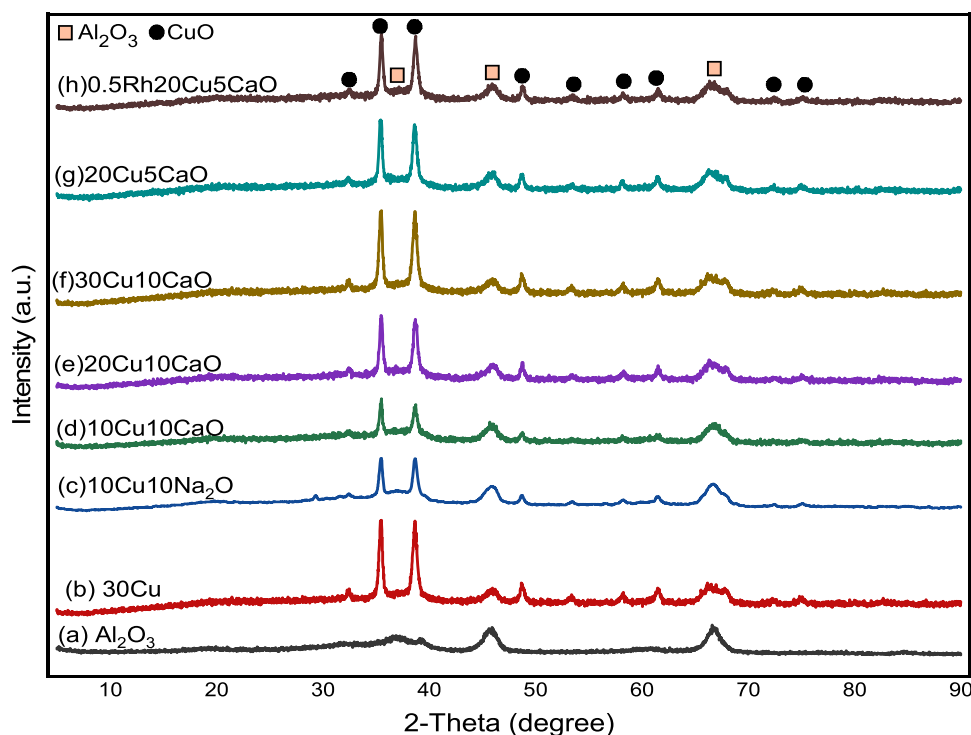


Fig. 4. XRD patterns of prepared catalysts, (a)  $\text{Al}_2\text{O}_3$ , (b) 30Cu (c)10Cu10 $\text{Na}_2\text{O}$ , (d)10Cu10CaO, (e) 20Cu10CaO, (f) 30Cu10CaO, (g) 20Cu5CaO, and (h) 0.5Rh20Cu5CaO.

### 3.1.3. X-ray photoelectron spectroscopic (XPS) of catalysts

The surface composition of copper species laying on the surface of the catalyst was investigated by XPS and the results are summarized in Table 3. Species analyses shown in Fig. 5 reveal that all synthesized catalysts displayed three  $\text{Cu}2p_{3/2}$  contributions, with their associated satellites visible in the range of 940.7–945.8 eV with the exception of 20Cu5CaO and 0.5Rh20Cu5CaO catalysts which showed only two  $\text{Cu}2p_{3/2}$  peaks. The split of the main photopeak into three contributions suggests the presence of three different Cu species, i.e., copper metal, copper oxides, and highly ionized and/or induced Cu species. Furthermore, shakeup satellite peaks were located at distances varying from 8 eV to 9.2 eV. According to Batista et al. only  $\text{Cu}^{2+}$  species show a shakeup satellite peak located about 10 eV higher than the  $\text{Cu}2p_{3/2}$  transition [35,36]; this characteristic peak is used to differentiate between  $\text{Cu}^{2+}$  and reduced copper. The observed peaks at higher binding energies could be attributed to the CuO moiety, while the lower binding energy peak could be assigned to the presence of  $\text{Cu}^{1+}$ , which is close to the one reported earlier for pure  $\text{Cu}_2\text{O}$  (932.8 eV). Fig. 5a represents the XPS spectra of catalysts containing different adsorbent types, namely, 10Cu10 $\text{Na}_2\text{O}$  and 10Cu10CaO. For both catalysts, the first  $\text{Cu}2p_{3/2}$  peaks correspond to  $\text{Cu}^{+2}$  ions in CuO and observed at 933.5 eV and

933.7 eV. The second and third peaks appearing at  $\text{Cu}2p_{3/2}$  and  $\text{Cu}2p_{1/2}$  were shifted to higher values of binding energy, indicating a stronger metal support interaction on the  $\text{Al}_2\text{O}_3$  support [37]. Fig. 5b shows the effects of copper loading on the surface chemical composition of the catalysts. For catalysts containing 10 wt% and 20 wt% Cu, the  $\text{Cu}2p_{3/2}$  composed of three combinations peaks falling in the region 933.5 eV and 933.9 eV. Their corresponding satellites are observed between 944.02 eV and 945.8 eV, which confirms the presence of CuO and phase out the presence of  $\text{Cu}_2\text{O}$ . However, a shift on  $\text{Cu}2p_{3/2}$  and  $\text{Cu}2p_{1/2}$  binding energy towards lower values was observed for the catalyst containing 30 wt%Cu, associated with lower satellite peaks, suggesting a lower metal-support interaction. Fig. 5c shows the effects of adsorbent loading on the chemical structure of the catalysts. There are two peaks in the core level region for 5% CaO, whereas with increase in the adsorbent loading to 10% CaO, one additional peak at higher binding energy was observed. The additional peaks of highly induced CuO species falling at binding energies of 939.5 eV and 958.1 eV, were assigned to the  $\text{Cu}2p_{3/2}$  and  $\text{Cu}2p_{1/2}$  signals, respectively. Fig. 5d depicts the core level photoelectron peaks of Cu2p for Rh-promoted and un-promoted 20Cu5CaO. As presented, the  $\text{Cu}2p_{3/2}$  and  $\text{Cu}2p_{1/2}$  signals are composed of two combination peaks with no significant difference in the binding energy values. However, with Rh promotion the peak intensity appearing at 935 eV increases thus indicating an increase in induced and/or strongly associated  $\text{Cu}^{2+}$  species.

Table 3

Location of the satellite,  $\text{Cu}2p_{3/2}$ ,  $\text{Cu}2p_{1/2}$ .

No.	Catalyst	Binding energy, eV			Satellite, eV
		Cu2p <sub>3/2</sub>			
		<sup>i</sup> Cu	<sup>ii</sup> Cu	<sup>iii</sup> Cu	
1	10Cu10Na <sub>2</sub> O	933.7	935.9	938.03	943.3
2	10Cu10CaO	933.5	937.7	941.16	945.8
3	20Cu10CaO	933.9	936.9	939.5	944.02
4	30Cu10CaO	932.1	933.9	936.1	941.4
5	20Cu5CaO	932.1	934.7	-	940.7
6	0.5Rh20Cu5CaO	932.4	934.8	-	941.1

Where;  $^i\text{Cu}$  = corresponds to metallic zerovalent copper,  $^{ii}\text{Cu}$  = corresponds to copper oxide,  $^{iii}\text{Cu}$  = highly ionized and/or induced copper species.

### 3.1.4. Reducibility of the catalysts

The reducibility test of the catalysts was investigated using  $\text{H}_2$ -TPR technique. Obtained thermograms are presented in Fig. 6. All catalysts containing CaO exhibited a narrow, nearly symmetrical reduction peak in the temperature range between 230°C and 259°C at the opposite of  $\text{Na}_2\text{O}$ -containing catalyst, which peak was observed at a temperature of 364°C. The monometallic 30Cu/ $\text{Al}_2\text{O}_3$  showed a sharp main peak centered at 236 °C attributed to the reduction of CuO to Cu. The 10Cu10CaO, 20Cu10CaO, and 30Cu10CaO catalysts reduction peaks situated at 245°C, 249°C, and 259°C, respectively. clearly show a rise in reduction temperature as copper content increases in the catalyst



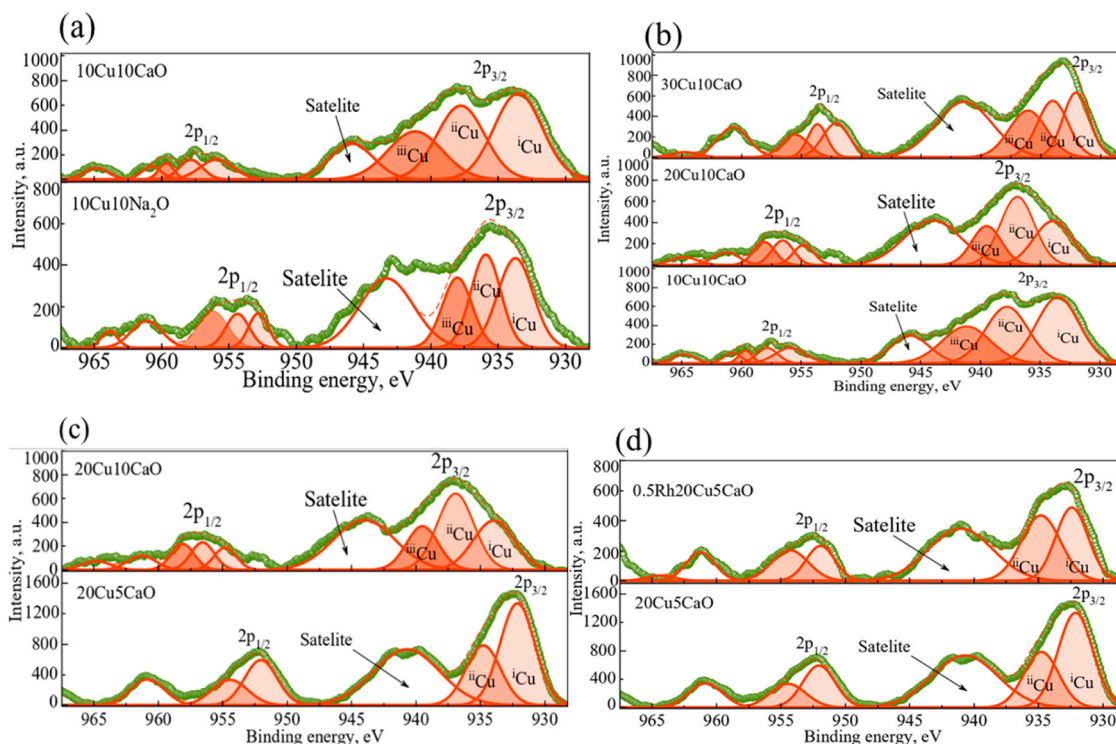


**Fig. 5.** Representative XPS of the Cu2p<sub>3/2</sub>, Cu2p<sub>1/2</sub> regions of (a) catalysts with different adsorbent types, (b) catalysts with varied Cu loading, (c) catalysts with varied adsorbent loading, and (d) Promoted and unpromoted catalysts.

composition. This, indicates that catalysts with low copper content had a good copper species dispersion at the opposite of catalysts with higher copper content, which tend to agglomerate into larger particles as the copper level increases, making the catalysts reduction more challenging and requiring higher reduction temperature. The porosity of synthesized catalysts may also be related to the rise of reduction temperature with increasing Cu content as porous materials require higher temperatures to be reduced [38]. The reduction of CuO is thought to occur in two steps, Cu<sup>2+</sup> gets reduced to Cu<sup>+</sup> first, which is subsequently reduced to zerovalent Cu<sup>0</sup> according to Eq. (10):



Previous research indicates that well-dispersed copper oxide species are reduced before bulk CuO species. Zhao et al. reported that the reduction peak for bulk CuO is located at about 380 °C [39], thus, the reduction peaks shown in Fig. 6 can be assigned to the reduction of CuO to Cu<sub>2</sub>O species. All samples displayed almost similar reduction pattern, the only difference was the presence of shoulder peak displayed for 20Cu5CaO (profile f). This peak situated at 520 °C was assigned to the reduction of Cu<sub>2</sub>O and well-dispersed CuO to Cu<sup>0</sup> [40] and to the strong interaction of Cu and defective sites of Al<sup>3+</sup> [41]. Comparing profile (d) to profile (f) of the two catalysts that contain similar copper content of 20% with different adsorbent loading of 10% and 5% CaO, respectively. It was observed that the catalyst with lower CaO content (5% CaO) had lower temperature reduction peak, which indicates that the interface of Cu/5%CaO has higher hydrogen spillover capacity compared to that for the catalyst with 10%CaO.

The reducibility of bimetallic copper catalysts can be improved by the addition of noble metals. Chang et al. compared the reducibility of CuO/ZnO/Al<sub>2</sub>O<sub>3</sub> before and after the addition of noble metals (Pd, Pt, Ru and Rh) and recorded a shift in the reduction peak to a lower temperature range in TPR profiles [42]. The obtained profile (g) from this work, shows the effect of addition of Rh noble metal on supported monometallic copper catalyst. The addition of Rh to 20Cu5CaO resulted in a shift of the reduction peaks observed in profile (e) ascribed to the

reduction of copper oxides species towards lower temperatures of 230 °C and 336 °C, respectively. This result implies that promoting copper-based catalysts by noble metals facilitates the reduction of 20Cu/5CaO catalyst. This result can be explained by the fact that the adsorbed H<sub>2</sub> can be easily dissociative to atomic hydrogen on the noble metals and then spilled over to the adjacent copper oxide species. These results are in good agreement with the findings of Mierczynski et al. [43] who investigated the effect of noble metals on the reducibility of copper-based catalysts and reported that promoting the catalysts with Rh enhances the reduction of Cu (II) oxide to Cu (I) and Cu (I) oxide to metallic Cu species.

### 3.1.5. H<sub>2</sub>-TPD and CO<sub>2</sub>-TPD analysis of the catalysts

The nature of the active sites on the surface of different catalysts was investigated using the analytical methods of H<sub>2</sub>-TPD and CO<sub>2</sub>-TPD, and the findings are displayed in Fig. 7. As can be seen in Fig. 7a(i), the 30-Cu-Al<sub>2</sub>O<sub>3</sub> catalyst displayed two hydrogen desorption peaks. First desorption peak in the temperature range of 50 °C to 140 °C attributed to the desorption of chemisorbed hydrogen from uniformly distributed and smaller copper species. The second broader peak covers a temperature range from 140 °C to approximately 380 °C, which might be associated with either stronger adsorbed hydrogen or hydrogen desorption from the bulk copper. It is noteworthy to point out that for the promoted Rh20Cu5CaO catalyst presented in Fig. 7a(iv), two distinct changes were observed compared to the 30Cu-Al<sub>2</sub>O<sub>3</sub> catalyst, firstly three hydrogen desorption peaks with maxima at temperature of 50 °C, 110 °C, and 220 °C were recorded. Secondly, a shift in the desorption temperature to lower degrees was noticed for the Rh-promoted catalyst proposing improved hydrogen desorption. In contrast, for the 10Cu10Na<sub>2</sub>O and 20Cu5CaO catalysts presented in Fig. 7a(ii) and 7a(iii) respectively, a high temperature desorption peak was also observed in the temperature range of 500 °C to 600 °C attributed to the desorption of strongly chemisorbed hydrogen atoms. Findings from the H<sub>2</sub>-TPD results were in good agreement with the H<sub>2</sub>-TPR analysis. As will be explained later, adding Rh to the catalysts improves their reducibility and



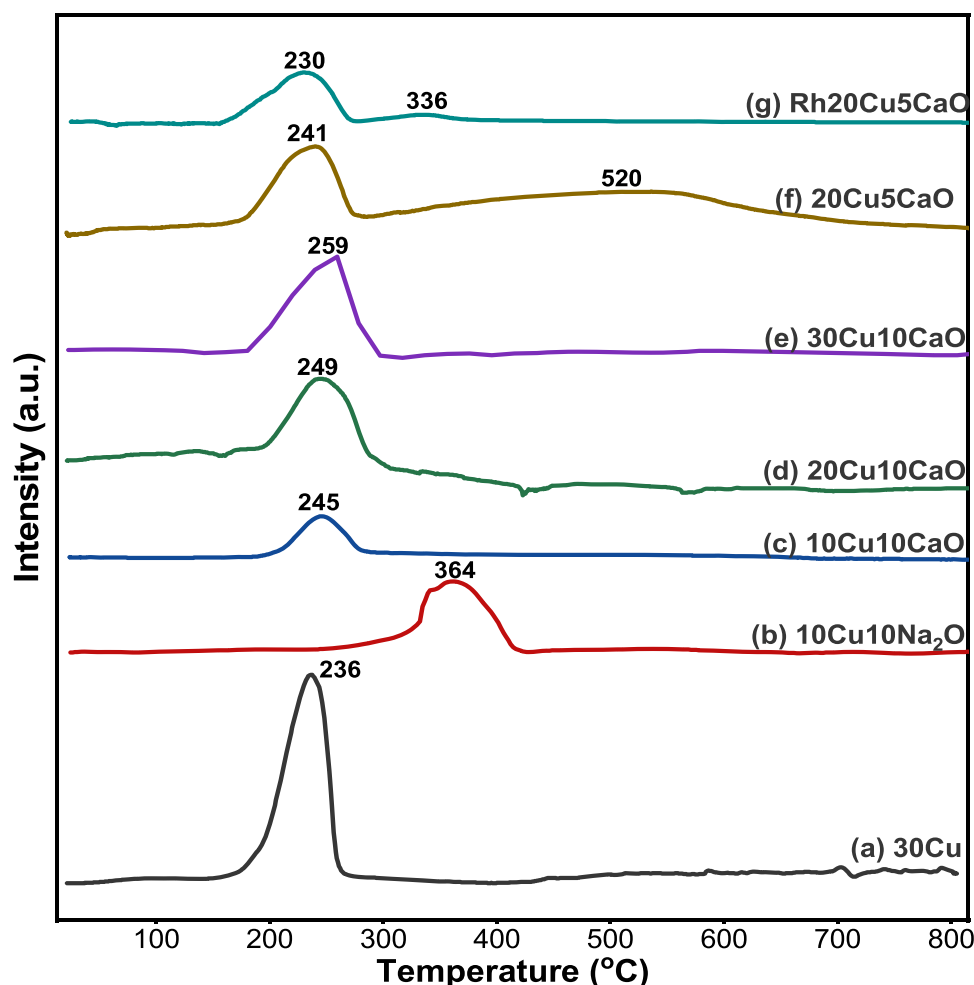


Fig. 6.  $H_2$ -TPR profile of the catalysts, (a) 30Cu (b) 10Cu10Na<sub>2</sub>O, (c) 10Cu10CaO, (d) 20Cu10CaO, (e) 30Cu10CaO, (f) 20Cu5CaO, and (g) 0.5Rh20Cu5CaO.

dispersion, and as a result, their catalytic performance by CO<sub>2</sub>-TPD technique is an essential tool for identifying the surface basic sites for CO<sub>2</sub> adsorption. CO<sub>2</sub>-TPD analysis was also performed for various catalysts and desorption thermograms are displayed in Fig. 7b. The desorption peaks can be categorized in three groups: weak basic sites, which occur below 200 °C, moderate basic sites, which occur between 300 °C and 600 °C, and strong basic sites, which occur at desorption temperatures higher than 600 °C. All catalysts exhibited weak to moderate basic sites, with the exception of the 10Cu10Na<sub>2</sub>O catalyst. There was an apparent rise in the desorption temperature for the 10Cu10Na<sub>2</sub>O catalyst towards higher degrees, but no notable desorption peaks were observed in the low temperature range. In comparison to the unpromoted 20Cu5CaO catalyst, the addition of the Rh-promoter resulted in only a slight modification in the desorption peaks to lower degrees. Weak and moderate basic sites appear to be beneficial to the methanol selectivity during the CO<sub>2</sub> hydrogenation process. The 10Cu10Na<sub>2</sub>O catalyst showed the lowest methanol selectivity, which may have been caused by the absence of weak basic and moderate basic sites, as will be covered in more detail in a later section. comparatively higher.

### 3.2. Reactor performance tests

#### 3.2.1. Effects of adsorbent type

The activity of the catalyst as well as the reaction mechanism are significantly influenced by the support and its interaction with the active metal. Particularly for CO<sub>2</sub> hydrogenation on Cu-based catalyst, the methanol formation sensitively depends on the nature of the support material and the presence of the additives [44]. In this study, the

influence of the 10 wt%Na<sub>2</sub>O and 10 wt%CaO as adsorbent on the performance of the catalysts was investigated under T= 300 °C, P= 60 bars, and GSHV of 5000 h<sup>-1</sup>. Fig. 8 shows the catalytic activity of 10Cu10Na<sub>2</sub>O and 10Cu10CaO catalysts. As shown in Fig. 8a, although no considerable difference in the percentage of CO<sub>2</sub> converted, noticeable differences in methanol selectivity and methanol yield were observed for the two catalysts. The obtained results showed that CaO-containing catalyst (10Cu10CaO) had higher selectivity towards methanol (15%) than Na<sub>2</sub>O-containing catalyst (10Cu10Na<sub>2</sub>O), which showed a negligible selectivity towards methanol (<1%) against a selectivity that almost reached 99% towards CO and produced around 0.427 g<sub>CO</sub>h<sup>-1</sup> g<sub>cat</sub><sup>-1</sup>. The relatively lower yields of methanol over the 10Cu10Na<sub>2</sub>O catalyst can be explained by the absence of effective hydrogen spill over to the active sites. As was shown by the H<sub>2</sub>-TPD tests results, the 10Cu10Na<sub>2</sub>O catalyst did not reveal the presence of weak and moderate hydrogen desorption peaks and the presence of strongly chemisorbed hydrogen presumably prevented hydrogen spill over to the active sites of CO<sub>2</sub> adsorption. These results were consistent with previously published reports [44]. These findings suggested that, in particular under these reaction conditions, Na<sub>2</sub>O adsorbent is not suitable for methanol synthesis from CO<sub>2</sub> conversion.

#### 3.2.2. Effects of adsorbent loading

An investigation on the effect of adsorbent (CaO) loading on the catalyst performance was performed in two different sets of experiments. In the first set, two different catalysts having the same copper loading of 20w% but different CaO loading of 10w% and 5w% denoted as 20Cu10CaO and 20Cu5CaO respectively and the results are

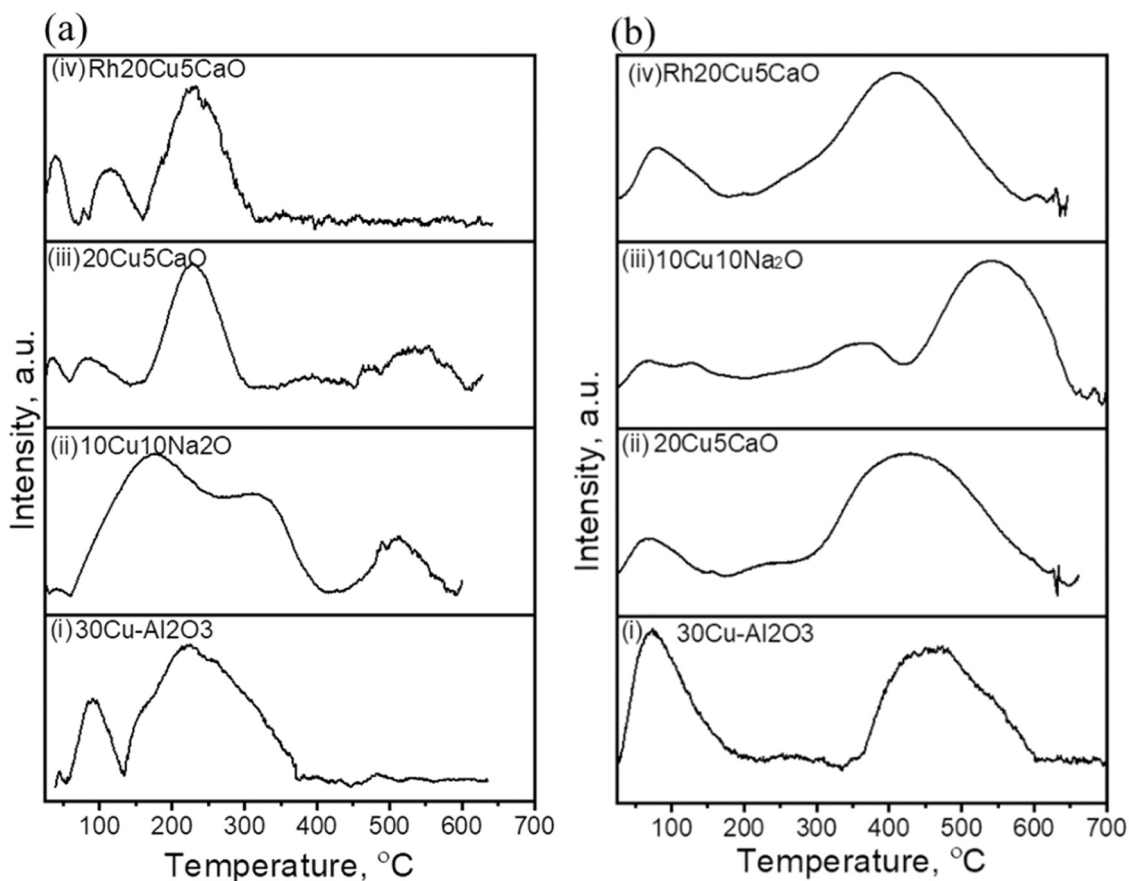


Fig. 7. Representing, (a)  $H_2$ -TPD and, (b)  $CO_2$ -TPD analysis results of the selected catalysts.

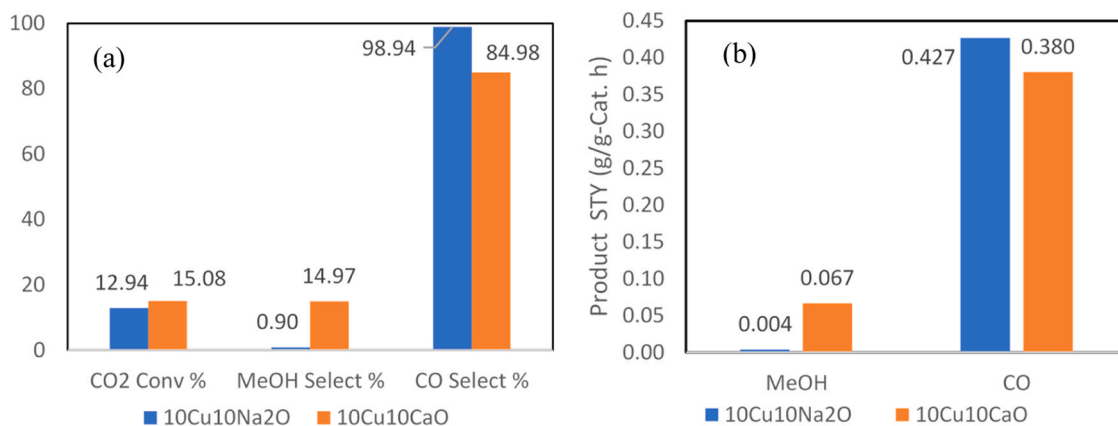
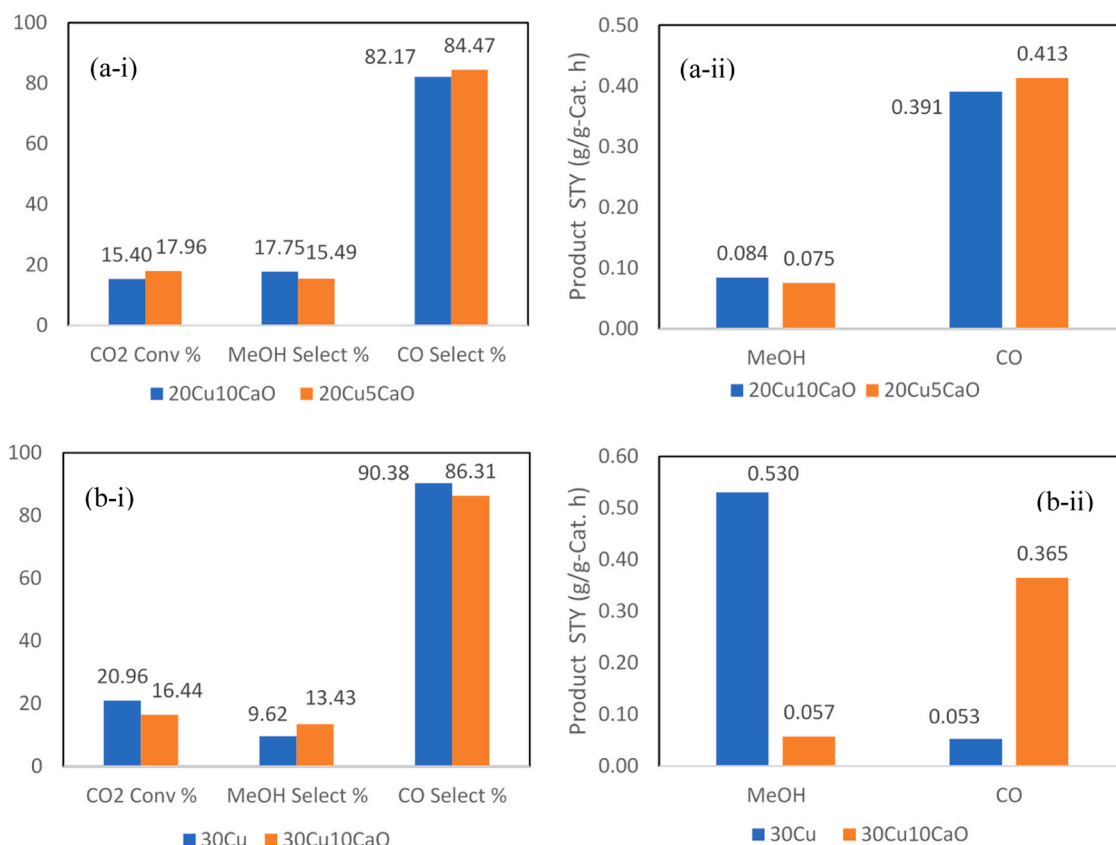


Fig. 8. Effects of adsorbent type on (a)  $CO_2$  conversion (%),  $CH_3OH$  selectivity (%) and CO selectivity, (b)  $CH_3OH$  yield ( $g_{CH_3OH} \cdot h^{-1} \cdot g_{cat}^{-1}$ ) and CO yield ( $g_{CO} \cdot h^{-1} \cdot g_{cat}^{-1}$ ).

presented in Fig. 9(a). In the second set, Fig. 9(b), two catalysts having the same Cu loading of 30wt%, one of them does not contain any adsorbent, while the second one contains 10wt% of CaO. Both sets of experiments were tested under the same operating conditions described earlier. As shown in Fig. 8(a), the  $CO_2$  conversion rose from 15.4% to 18% when the of the adsorbent decreased from 10 wt% to 5 wt% in the first set of experiment, while in the second set (Fig. 9b), the same phenomenon was observed where  $CO_2$  conversion decreased from 20.96% to 16.44% with CaO loading increased from 0wt% to 30wt%. Therefore, it appears that increased CaO loading had a negative impact of  $CO_2$  conversion. In fact,  $CO_2$  adsorption and its subsequent conversion to methanol can be explained by the fact that both copper active sites and adsorbent contribute to the overall performance of the catalysts.  $CO_2$  is

easily absorbed by CaO compared to copper, while hydrogen is thought to be chemisorbed and spilled over by the copper active sites. Hence, taking the case of 20Cu10CaO against 20Cu5CaO catalyst, it is reasonable to assume that the 20Cu10CaO catalyst has relatively reduced conversion is due to the stronger interaction between  $CO_2$  and the adsorbent, which prevents  $CO_2$  from being available for the reaction. Additionally, as was revealed by the  $CO_2$ -TPD and  $H_2$ -TPD analysis results, the increased presence of excess adsorbent at high CaO loading resulted in an increase in strong basic sites and strongly chemisorbed hydrogen and presumably made making  $CO_2$  desorption and hydrogen spill over onto metallic sites more challenging.

The effect of adsorbent loading on both methanol and CO selectivity was also assessed. From Fig. 8a, we observe that methanol selectivity



**Fig. 9.** Effect of adsorbent loading on CO<sub>2</sub> conversion and products selectivity over copper-based catalysts containing 20% Cu (a-i) and 30%Cu (b-i) and the corresponding products yield over 20% Cu (b-ii); and 30% Cu (b-ii) catalysts.

increased from 15.49% to 17.75% for CaO loading increasing from 5 wt % to 10 wt% while the opposite trend was obtained for CO selectivity which decreased from 84.47% to 82.17% for the same CaO loadings. These trends were further confirmed in Fig. 9b for catalysts containing 30% copper where methanol selectivity increased from 9.62% to 13.43% for CaO loading increasing from 0 wt% to 30 wt% against a decrease in CO selectivity from 90% to 82% for the same adsorbent loadings. Methanol and CO space time yields (STY) were also assessed as function of the adsorbent loading. As shown in Fig. 9(a), a small decrease in the STY of methanol was observed for the catalyst containing 5 wt% adsorbent loading against that containing 10 wt% adsorbent as it decreases from 0.084 gMeOH/g.cat.h with 20Cu10CaO catalyst to 0.075 gMeOH/g.cat.h in the case 20Cu5CaO. The same trend was observed in Fig. 8(b) for 30Cu and 30Cu10CaO catalyst where methanol selectivity increased from 0.053 gMeOH/g.cat.h to 0.057 gMeOH/g.cat.h. As for the yield (STY) for CO, the opposite behavior was observed for both sets of catalysts, where the CO yield decreases with increased CaO loading (Fig. 9, (a, b)).

### 3.2.3. Effects of Cu loading

Copper content is one of the most important elements influencing the activity of Cu-based catalysts in conventional methanol synthesis process. The amount of copper is closely related to the dispersion of metallic Cu, which serves as a primary active site for methanol synthesis. The referenced literature states that Cu-Al<sub>2</sub>O<sub>3</sub> catalysts have been employed to produce methanol from CO<sub>2</sub> in the temperature range of 282–487 °C and pressure range of 117–410 atm. At 285 °C and 410 atm, catalysts with a Cu concentration of 8–25% were the most active ones [45]. Kim et al. [46] investigated the effect of varying Cu content from 30 wt% to 70 wt%, and reported that catalyst with 50 wt% Cu exhibited the highest activity for methanol synthesis. In our work, four different catalysts with Cu compositions of 0 wt%, 10 wt%, 20 wt%, and 30 wt%

impregnated on a similar base material of 10% CaO/ $\gamma$ -Al<sub>2</sub>O<sub>3</sub> were synthesised and tested for methanol synthesis under reaction conditions of T = 300 °C, P = 60 bars, GHSV = 5000 h<sup>-1</sup> and CO<sub>2</sub>:H<sub>2</sub> ratio of 3:1. The catalysts' performances evaluated in terms of CO<sub>2</sub> conversion, methanol selectivity and yield, and carbon monoxide selectivity and yield are presented in Fig. 10.

The effect of Cu content on the catalytic performance of developed catalysts was investigated using three different catalysts with variable Cu content of 10 wt%, 20 wt% and 30 wt% (Fig. 10). Obtained results showed a small increase in converted CO<sub>2</sub> ranging from 15.08% to 16.44% for catalysts containing 10 wt% and 30 wt% of Cu respectively, while 20 wt% catalyst had a CO<sub>2</sub> conversion of 15.44%.

The effect of Cu content on CO<sub>2</sub> conversion is related to Cu surface area, its dispersion, as well as the confined crystallization of copper nanoparticles. The increased CO<sub>2</sub> conversion with increased Cu content in the catalysts can be ascribed to increased fraction of CuO on the metal support as revealed by XRD analysis, providing more Cu surface area. The CO<sub>2</sub> conversion might also be attributed to the catalyst support (10CaO/Al<sub>2</sub>O<sub>3</sub>) and its interface effect with Cu metal. It is well known that the base material is a dominant factor that directly influences the reaction activity, which is basically achieved by forming a metal-support interface or active metal-support interaction [47] as the support material (10CaO/Al<sub>2</sub>O<sub>3</sub>) immobilized Cu particles, which accordingly, enhances the active site dispersion and maintained high thermal stability. Furthermore, the strong metal-support interaction causes high synergy which, results in higher reactivity of the elementary surface reaction, especially when the support adsorb then transfers the reactants to the active sites without being involved in the reaction [48]. Moreover, higher Cu loading affects the amount of CO<sub>2</sub> adsorbed, suggesting that the formed CuO has basic sites to adsorb CO<sub>2</sub>. In other words, increasing Cu concentration possibly increased the presence of the interfaces between Cu and adsorbent dispersed around Al<sub>2</sub>O<sub>3</sub> support. A similar

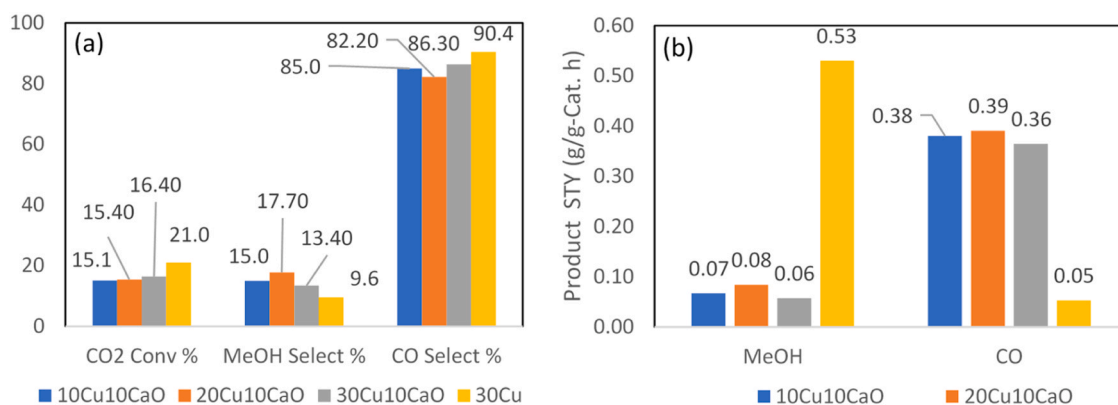


**Fig. 10.** Effects of Cu loading on (a) CO<sub>2</sub> conversion (%), CH<sub>3</sub>OH selectivity (%) and CO selectivity, (b) CH<sub>3</sub>OH yield (g<sub>CH<sub>3</sub>OH</sub> h<sup>-1</sup>.g<sub>cat</sub><sup>-1</sup>) and CO yield (g<sub>CO</sub>.h<sup>-1</sup>.g<sub>cat</sub><sup>-1</sup>) in different catalysts.

phenomenon was observed by Din et al. [49], who investigated the activity of Cu/Zr/CNF catalyst containing 15 wt% Cu at 3 MPa and obtained a CO<sub>2</sub> conversion of 11%. Witton et al. [50] investigated CO<sub>2</sub> hydrogenation to methanol over Cu/ZO<sub>2</sub>, containing 10 wt% Cu synthesized by the same preparation method as in this work at reaction conditions of T=220–300 °C and P= 30 bars and obtained a CO<sub>2</sub> conversion in the range of 3–13%.

Methanol selectivity and methanol space time yield (STY) as a function of Cu loading are presented in Fig. 10. Under identical reaction conditions, it was found that methanol selectivity increased with increased Cu loading from 10 wt% to 20 wt% then decreased with the catalyst of 30 wt% Cu loading in. A similar trend was observed for methanol STY (g<sub>CH<sub>3</sub>OH</sub> h<sup>-1</sup>.g<sub>cat</sub><sup>-1</sup>). Catalyst impregnated with 20 wt% Cu had the highest methanol selectivity (17.75%) and STY (0.084 g<sub>MeOH</sub>.cat<sup>-1</sup>.h<sup>-1</sup>), while catalyst containing a Cu loading of 30 wt % had the lowest methanol selectivity and STY of 13.4% and 0.057 g<sub>MeOH</sub> cat<sup>-1</sup> h<sup>-1</sup>, respectively. The catalyst with 10 wt% copper had methanol selectivity of 14.47% and STY of 0.067 g<sub>MeOH</sub> cat<sup>-1</sup> h<sup>-1</sup>. The material activity and methanol selectivity are affected by the copper amount that is correlated to the metal oxide particle size. The catalyst with lower copper loading of 10 wt% had the smallest metal oxide nanoparticles on the surface (8.1 nm) as reported by TEM analysis. Hence, it facilitates the reverse water-gas shift reaction, limiting the formation of methanol and reducing its selectivity. the decrease in methanol selectivity and STY with Cu loading of 30 wt% might be attributed to the resulting copper sintering at the catalyst's surface and agglomeration and accumulation of copper particles which are in agreement with the findings reported by Karelavic et al. [51]. Moreover, the enhanced methanol selectivity with the catalyst containing 20 wt% Cu might also be attributed to the suppressing of reverse water gas shift reaction, which decreases the CO selectivity and increases methanol synthesis. The TEM results showed that the catalysts containing 10 wt% Cu and 30 wt% Cu have close sizes of metal oxide particles, which explains the close results in terms of methanol selectivity and yield. This finding was confirmed by Liu et al. who reported a superior reactivity and maximum methanol selectivity with Cu-containing particles of sizes varying between 8 and 10 nm [44]. The methanol synthesis performance using catalysts containing varied Cu loadings can be explained in terms of the nature of Cu species given by XPS analysis. Increasing the metallic loading to 20 wt% in 20Cu10CaO enhanced the production of CH<sub>3</sub>OH and the selectivity towards it. In this sample, even though the surface area was reduced to 107.29 m<sup>2</sup>/g but this reduction was compensated by the dominant presence of Cu<sup>+</sup> in higher amount compared to other samples.

Selectivity and STY of CO were relatively high and followed exactly opposite trends to that of methanol. The CO selectivity and STY attained their lowest values of 82.17% and 0.0391 (g<sub>CO</sub>.h<sup>-1</sup>.g<sub>cat</sub><sup>-1</sup>) for 20Cu10CaO

catalyst followed by 84.98% and 0.380 (g<sub>CO</sub>.h<sup>-1</sup>.g<sub>cat</sub><sup>-1</sup>) obtained with 10Cu10CaO catalyst. and while a selectivity of 86.31% and a STY of 0.365 (g<sub>CO</sub>.h<sup>-1</sup>.g<sub>cat</sub><sup>-1</sup>) was obtained for 30Cu10CaO catalyst., respectively.

### 3.2.4. Promoter effect on the catalyst performance

The effect of incorporating a catalytic promoter on the catalytic performance of the synthesized catalysts was assessed by selecting the best performing catalyst and adding a noble metal. Since 20Cu10CaO catalyst displayed the highest overall performance, 0.5 wt.% of Rhodium was added to further increase the material's activity and increase its selectivity towards methanol. Fig. 11 demonstrates that while CO<sub>2</sub> conversion dropped from 17.96% to 13.78 with the incorporation of Rh into 20Cu10CaO catalyst, MeOH selectivity drastically rose to around 23.2% with the promoter from 15.49% initially obtained without promoter while the STY increased from 0.075 to 0.081 (g<sub>CH<sub>3</sub>OH</sub> h<sup>-1</sup>.g<sub>cat</sub><sup>-1</sup>). The opposite trend was obtained for CO formation where it selectivity decreased from 84.47% to 76.76% and STY from 0.413 without promoter to 0.305 (g<sub>CO</sub>.h<sup>-1</sup>.g<sub>cat</sub><sup>-1</sup>) with promoter. The obtained results were similar to the results patterns reported in the open literature [52] which suggested that Rh-supported material provides sufficient reactions sites owing to the enhanced exposure of reactants to the catalyst particles and the associated magnificent surface properties.

### 3.2.5. Postulated mechanism of CO<sub>2</sub> hydrogenation to methanol

There remains a debate over the mechanism that drives the CO<sub>2</sub> hydrogenation to methanol in the presence of heterogeneous catalysts, which is influenced by a wide range of factors. Nonetheless, as Fig. 12 illustrates, the scientific community has largely proposed and accepted two molecular pathways: the direct methanol synthesis route and the indirect methanol synthesis route. The formate pathway, often referred to as the direct route, is characterized by the accumulation of formate (-HCOO\*) intermediates, which are subsequently hydrogenated to produce methanol. On the contrary, according to the indirect route also known as the reverse water gas shift reaction (RWGS) route, the -CO\* radicals are produced at first step which are hydrogenated to methanol [17–21]. The later pathway is also more conducive to the production of byproducts like methane and CO. As demonstrated in Fig. 12, a dual-site catalyst is necessary for CO<sub>2</sub> hydrogenation reaction. The chemisorption and dissociation of hydrogen require metallic active sites (Cu in the reported work), whereas CO<sub>2</sub> must be chemisorbed on the second active site (Na<sub>2</sub>O and CaO in this reported work). An effective hydrogen spill over mechanism will result in the production of more -HCOO\* radicals, and subsequent hydrogenation will increase the yield of methanol. This makes hydrogen spill over from the copper surface to active sites where CO<sub>2</sub> is chemisorbed a limiting step after chemisorption of the reactive species. On the contrary, additional -CO\* radicals will be produced if



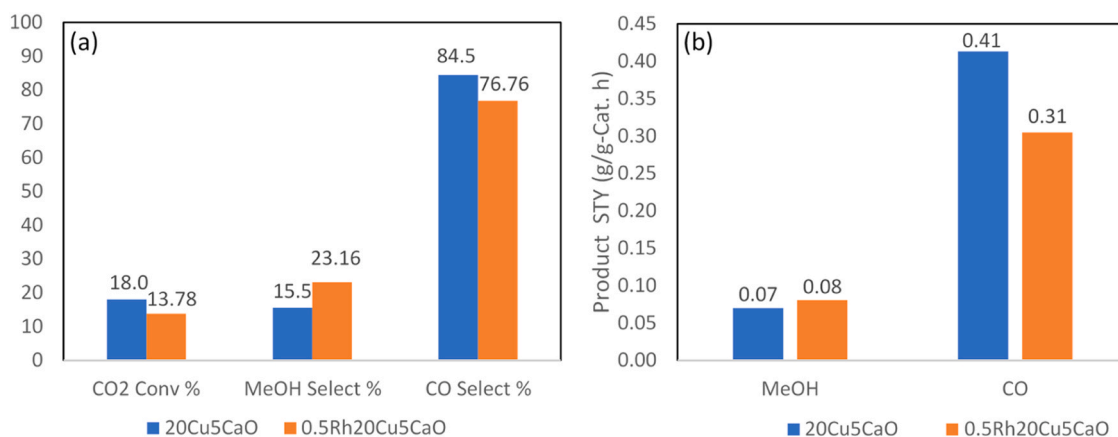


Fig. 11. Effect of promoting (a) CO<sub>2</sub> conversion (%), CH<sub>3</sub>OH selectivity (%) and CO selectivity, (b) CH<sub>3</sub>OH yield (gCH<sub>3</sub>OH h<sup>-1</sup>·g<sub>cat</sub><sup>-1</sup>) and CO yield (gCO·h<sup>-1</sup>·g<sub>cat</sub><sup>-1</sup>).

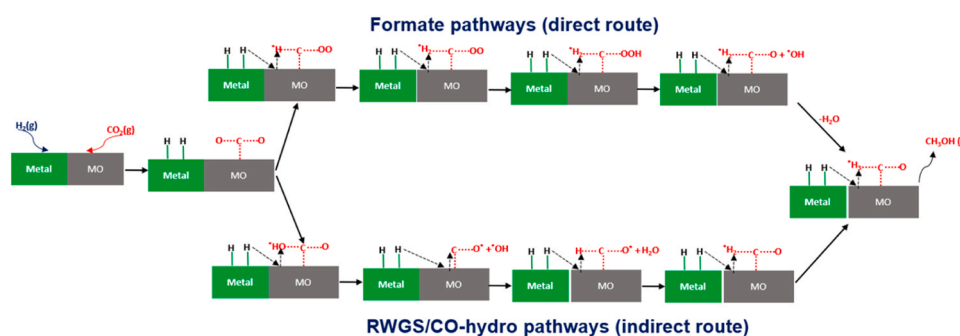


Fig. 12. Illustration of the dual-site reaction pathway of CO<sub>2</sub> hydrogenation reaction in presence of heterogeneous catalyst. **Note:** In illustration presented above, Metal = Cu, MO = Na<sub>2</sub>O/CaO.

there is either no spillover or inadequate hydrogen spillover, which will make the catalyst selective for CO or CH<sub>4</sub> instead of CH<sub>3</sub>OH. The TPR, CO<sub>2</sub>-TPD and H<sub>2</sub>-TPD analysis results support the hypothesis that the catalyst containing Na<sub>2</sub>O and having a composition of 10Cu10Na<sub>2</sub>O follows the RWGS pathway since there is no effective hydrogen spill over. Contrary to this, due to its efficient hydrogen spill over, the 20Cu5CaO catalyst efficiently follows the formate route. It is therefore reasonable to conclude that incorporating Rh to the CaO-containing samples enhanced hydrogen spillover and increased methanol production further.

#### 4. Conclusions

The objective of this study was to assess the viability of adding some adsorbents into catalysts support for CO<sub>2</sub> conversion methanol and other useful products. For this purpose, a series of novel Cu-based catalysts with Na<sub>2</sub>O and CaO adsorbents supported on alumina were synthesized characterized and evaluated in CO<sub>2</sub> hydrogenation reaction. The synthesized catalysts were thoroughly characterized by various analytical techniques and tested for their catalytic activity in a high-pressure packed bed reactor. The freshly prepared catalysts were initially screened under fixed conditions of T=300 °C, P=60 bars, and GHSV=5000 h<sup>-1</sup>. The screening tests showed that the nature of the adsorbent significantly affects the performance of the catalysts. Although the CO<sub>2</sub> conversion of the 10Cu10Na<sub>2</sub>O catalyst was greater than that of 10Cu10CaO catalyst, the Na<sub>2</sub>O-containing catalyst negligible selectivity to methanol. This is probably because Na<sub>2</sub>O has a significant hydrogen adsorption capacity, which limits hydrogen spillover the active site. Hence, Na<sub>2</sub>O-containing catalysts have been discarded from further investigation and only CaO-containing catalysts have been further investigated. Three different catalysts with fixed CaO content of

10 wt% and variable Cu content of 10 wt%, 20 wt% and 30 wt% resulted in a small increase in CO<sub>2</sub> conversion varying between a minimum of 15.08% and a maximum of 16.44% obtained with 20Cu10CaO associated with the highest methanol selectivity (17.75%) and STY (0.084 g<sub>MeOH</sub>·cat<sup>-1</sup>·h<sup>-1</sup>), while catalyst containing a Cu loading of 30 wt % had the lowest methanol selectivity and STY of 13.4% and 0.057 g<sub>MeOH</sub> cat<sup>-1</sup> h<sup>-1</sup>, respectively.

Reducing CaO content to 5 wt% boosted the CO<sub>2</sub> conversion to 17.96%; however, the sample had higher selectivity towards CO rather than methanol compared to the catalysts containing 10%CaO. However, complete removal of CaO from copper-based catalyst (30Cu) further increased the CO<sub>2</sub> conversion to 20.96% from 16.44 but decreased the methanol selectivity from 13.43% to 9.62%. The best performing catalyst in term of CO<sub>2</sub> conversion (20Cu5CaO) was further promoted with 0.5% Rh, which resulted in improved CH<sub>3</sub>OH selectivity and yield of 23.2% and 0.08 g<sub>MeOH</sub>·cat<sup>-1</sup>·h<sup>-1</sup>, respectively. The comparatively higher performance of the Rh-promoted catalyst was attributed to the existence of highly dispersed, small copper oxide nanoparticles that are strongly interacting with the supports as well as the presence of induced phases.

#### CRediT authorship contribution statement

**Rim Ismail:** Investigation, Data curation. **Muftah El-Naas:** Writing – review & editing, Visualization, Conceptualization. **Ahmed Soliman:** Validation, Formal analysis, Data curation. **Abdelbaki Benamor:** Writing – review & editing, Supervision, Project administration. **Mohamed J. Al-Marri:** Writing – original draft, Validation, Conceptualization. **Mohamed Ali H. Saad:** Writing – original draft, Formal analysis, Conceptualization. **Ali Sardar:** Resources, Methodology, Formal analysis. **Assem T. Mohamed:** Writing – original draft, Investigation, Formal analysis, Data curation.

## Declaration of Competing Interest

The authors declare that they have no known competing financial interests or personal relationships that could have appeared to influence the work reported in this paper.

## Data availability

Data will be made available on request.

## Acknowledgments

This work possible through Qatar University internal grant # IRCC 2023–203. Special thanks go to the CLU staff for their help in providing timely sample analysis. Open Access funding provided by the Qatar National Library.

## Appendix A. Supporting information

Supplementary data associated with this article can be found in the online version at doi:10.1016/j.jece.2024.112325.

## References

- [1] I. Khan, et al., World energy trilemma and transformative energy developments as determinants of economic growth amid environmental sustainability 108 (2022) 105884.
- [2] P. Renforth, G.J.Ro.G. Henderson, Assessing ocean alkalinity for carbon sequestration 55 (3) (2017) 636–674.
- [3] G.P. Peters, et al., The challenge to keep global warming below 2 C 3 (1) (2013) 4–6.
- [4] Schneider, S., et al., Overview of impacts, adaptation, and vulnerability to climate change. 2001: p. 75–103.
- [5] K. Haustein, et al., A real-time global warming index 7 (1) (2017) 15417.
- [6] X. Jiang, et al., Recent advances in carbon dioxide hydrogenation to methanol via heterogeneous catalysis 120 (15) (2020) 7984–8034.
- [7] J. Zhang, et al., Highly active and selective electrocatalytic CO<sub>2</sub> conversion enabled by core/shell Ag/(amorphous-Sn (IV)) nanostructures with tunable shell thickness 11 (43) (2019) 39722–39727.
- [8] T.P. Nguyen, et al., Recent advances in TiO<sub>2</sub>-based photocatalysts for reduction of CO<sub>2</sub> to fuels 10 (2) (2020) 337.
- [9] M.J.C. Bowker, Methanol synthesis from CO<sub>2</sub> hydrogenation 11 (17) (2019) 4238–4246.
- [10] J.-L. Dubois, K. Sayama, H.J.Cl Arakawa, Conversion of CO<sub>2</sub> to dimethylether and methanol over hybrid catalysts 21 (7) (1992) 1115–1118.
- [11] R. Ullah, et al., Adsorption equilibrium studies of CO<sub>2</sub>, CH<sub>4</sub> and N<sub>2</sub> on various modified zeolites at high pressures up to 200 bars 262 (2018) 49–58.
- [12] J. Rogacka, et al., High-throughput screening of metal–organic frameworks for CO<sub>2</sub> and CH<sub>4</sub> separation in the presence of water 403 (2021) 126392.
- [13] J. Serafin, et al., Highly microporous activated carbons from biomass for CO<sub>2</sub> capture and effective micropores at different conditions 18 (2017) 73–79.
- [14] H. Zhao, et al., Carbon-based adsorbents for post-combustion capture: a review 8 (1) (2018) 11–36.
- [15] R.S. Liu, et al., Advances in post-combustion CO<sub>2</sub> capture by physical adsorption: from materials innovation to separation practice 14 (6) (2021) 1428–1471.
- [16] K.H. Chai, et al., Effect of CO<sub>2</sub> adsorbents on the Ni-based dual-function materials for CO<sub>2</sub> capturing and in situ methanation 67 (6) (2020) 998–1008.
- [17] A. Bermejo-López, et al., Ni loading effects on dual function materials for capture and in-situ conversion of CO<sub>2</sub> to CH<sub>4</sub> using CaO or Na<sub>2</sub>CO<sub>3</sub> 34 (2019) 576–587.
- [18] E.T. Gall, et al., Investigating CO<sub>2</sub> removal by Ca- and Mg-based sorbents with application to indoor air treatment 110 (2016) 161–172.
- [19] I. Hinkov, , 2016, Carbon dioxide capture by adsorption. 2016. 51(6): p. 609–626..
- [20] C.J. Keturakis, et al., Monitoring solid oxide CO<sub>2</sub> capture sorbents in action 7 (12) (2014) 3459–3466.
- [21] M.A. Arellano-Treviño, et al., Catalysts and adsorbents for CO<sub>2</sub> capture and conversion with dual function materials: Limitations of Ni-containing DFMs for flue gas applications 31 (2019) 143–151.
- [22] H. Sun, et al., Progress in the development and application of CaO-based adsorbents for CO<sub>2</sub> capture—a review 1 (2018) 1–27.
- [23] A.A.G. Belova, T.M. Yegulalp, C.T.J.E.P. Yee, Feasibility study of In Situ CO<sub>2</sub> capture on an integrated catalytic CO<sub>2</sub> sorbent for hydrogen production from methane 1 (1) (2009) 749–755.
- [24] M.S. Duyar, et al., In situ CO<sub>2</sub> capture using CaO/γ-Al<sub>2</sub>O<sub>3</sub> washcoated monoliths for sorption enhanced water gas shift reaction 53 (3) (2014) 1064–1072.
- [25] X.-M. Liu, et al., Recent advances in catalysts for methanol synthesis via hydrogenation of CO and CO<sub>2</sub> 42 (25) (2003) 6518–6530.
- [26] P. Gao, et al., Fluorinated Cu/Zn/Al/Zr hydrotalcites derived nanocatalysts for CO<sub>2</sub> hydrogenation to methanol 16 (2016) 32–41.
- [27] J. Kim, et al., Catalytic ozonation of toluene using Mn–M bimetallic HZSM-5 (M: Fe, Cu, Ru, Ag) catalysts at room temperature 397 (2020) 122577.
- [28] Q. Wu, et al., Current advances in bimetallic catalysts for carbon dioxide hydrogenation to methanol 313 (2022) 122963.
- [29] F.M. Berndt, O.W.J.R.K. Perez-Lopez, Catalytic decomposition of methane over Ni/ SiO<sub>2</sub>: influence of Cu addition, Mech., Catal. 120 (2017) 181–193.
- [30] Á.B. Sifontes, et al., Preparation of functionalized porous nano-γ-Al<sub>2</sub>O<sub>3</sub> powders employing colophony extract 4 (2014) 21–29.
- [31] M. Urbonavicius, et al., Production of gamma alumina using plasma-treated aluminum and water reaction byproducts 13 (6) (2020) 1300.
- [32] S. Suresh, et al., FTIR and multivariate analysis to study the effect of bulk and nano copper oxide on peanut plant leaves 1 (3) (2016) 343–350.
- [33] C. Torres, S. Rostom, H.J.C. de Lasa, An Eco-Friendly Fluidizable Fe x O y/CaO-γ-Al<sub>2</sub>O<sub>3</sub> Catalyst for Tar Cracking during Biomass Gasification 10 (7) (2020) 806.
- [34] N. Pasupulety, et al., Production of biodiesel from soybean oil on CaO/Al<sub>2</sub>O<sub>3</sub> solid base catalysts 452 (2013) 189–202.
- [35] J. Batista, et al., XPS and TPR examinations of γ-alumina-supported Pd-Cu catalysts 206 (1) (2001) 113–124.
- [36] S. Ali, et al., Development of highly active Cu-based CO<sub>2</sub> hydrogenation catalysts by solution combustion synthesis (SCS): Effects of synthesis variables 172 (2022) 106543.
- [37] N.A.M. Zabidi, T.S. Tuan Sulong, S. Ali, Synthesis and characterization of Cu/ZnO catalyst on carbon nanotubes and Al<sub>2</sub>O<sub>3</sub> supports, Mater. Sci. Forum (2018) (Trans Tech Publ).
- [38] M.I. Magzoub, et al., Utilization of steel-making dust in drilling fluids formulations 8 (5) (2020) 538.
- [39] Y. Zhao, K. Tao, H.L.J.C.C. Wan, Effect of zirconia phase on the reduction behaviour of highly dispersed zirconia-supported copper oxide 5 (5) (2004) 249–252.
- [40] B. Zhang, et al., Effect of copper loading on texture, structure and catalytic performance of Cu/SiO<sub>2</sub> catalyst for hydrogenation of dimethyl oxalate to ethylene glycol 21 (5) (2012) 563–570.
- [41] T. Zhu, et al., Hydrodeoxygenation of Benzofuran over Bimetallic Ni-Cu/γ-Al<sub>2</sub>O<sub>3</sub> Catalysts, Catalysts 10 (2020), <https://doi.org/10.3390/catal10030274>.
- [42] C.-C. Chang, et al., Effect of noble metal on oxidative steam reforming of methanol over CuO/ZnO/Al<sub>2</sub>O<sub>3</sub> catalysts 37 (15) (2012) 11176–11184.
- [43] P.J.C.L. Mierczynski, Comparative Studies of Bimetallic Ru–Cu, Rh–Cu, Ag–Cu, Ir–Cu Catalysts Supported on ZnO–Al<sub>2</sub>O<sub>3</sub>, ZrO<sub>2</sub>–Al<sub>2</sub>O<sub>3</sub> Systems 146 (2016) 1825–1837.
- [44] H. Liu, et al., Efficient production of methanol and diols via the hydrogenation of cyclic carbonates using copper–silica nanocomposite catalysts 17 (8) (2015) 4281–4290.
- [45] V. Ipatieff, G.J.JotA.C.S. Monroe, Synthesis of methanol from carbon dioxide and hydrogen over copper-alumina catalysts. Mechanism of reaction 67 (12) (1945) 2168–2171.
- [46] I. Kim, et al., Bifunctionality of Cu/ZnO catalysts for alcohol-assisted low-temperature methanol synthesis from syngas: Effect of copper content 26 (3) (2017) 373–379.
- [47] K. Stangeland, et al., Tuning the interfacial sites between copper and metal oxides (Zn, Zr, In) for CO<sub>2</sub> hydrogenation to methanol 238 (2021) 116603.
- [48] V. Deerattrakul, et al., The roles of nitrogen species on graphene aerogel supported Cu–Zn as efficient catalysts for CO<sub>2</sub> hydrogenation to methanol 580 (2019) 46–52.
- [49] I.U. Din, et al., Carbon nanofibers based copper/zirconia catalysts for carbon dioxide hydrogenation to methanol: Effect of copper concentration 334 (2018) 619–629.
- [50] T. Witton, et al., CO<sub>2</sub> hydrogenation to methanol over Cu/ZrO<sub>2</sub>catalysts: Effects of zirconia phases 293 (2016) 327–336.
- [51] A. Karelovic, P.J.C.S. Ruiz, The role of copper particle size in low pressure methanol synthesis via CO<sub>2</sub> hydrogenation over Cu/ZnO catalysts, Technology 5 (2) (2015) 869–881.
- [52] S. Rönisch, et al., Review on methanation—From fundamentals to current projects 166 (2016) 276–296.